The ^{13}C Pocket Strucure in AGB Models:

Constraints from Zirconium Isotope Abundances in Single Mainstream Grains

Nan Liu,[1,2,3] Roberto Gallino,[4] Sara Bisterzo,[4,5] Andrew M. Davis,[1,2,6]
Michael R. Savina,[2,3] Michael J. Pellin,[1,2,3,6]

[1]Department of the Geophysical Sciences, University of Chicago, Chicago, IL, 60637, USA

[2]Chicago Center for Cosmochemistry, Chicago, IL 60637, USA

[3]Materials Science Division, Argonne National Laboratory, Argonne, IL 60439, USA

[4]Dipartimento di Fisica, Università di Torino, Torino I-10125, Italy

[5]INAF−Osservatorio Astrofisico di Torino−Strada Osservatorio 20, Pino Torinese 10025, Italy;

[6]Enrico Fermi Institute, University of Chicago, Chicago, IL 60637, USA

January 2014

Submitted to: Astrophysical Journal Letters

The Astrophysical Journal Letters

THE ^{13}C POCKET STRUCTURE IN AGB MODELS: CONSTRAINTS FROM ZIRCONIUM ISOTOPE ABUNDANCES IN SINGLE MAINSTREAM GRAINS

NAN LIU [1,2,3], ROBERTO GALLINO [4], SARA BISTERZO [4,5],

ANDREW. M. DAVIS [1,2,6], MICHAEL R. SAVIN [2,3], MICHAEL J. PELLIN [1,2,3,6].

[1]Department of the Geophysical Sciences, The University of Chicago, Chicago, IL, 60637, USA; lnsmile@uchicago.edu;

[2]Chicago Center for Cosmochemistry, Chicago, IL 60637, USA;

[3]Materials Science Division, Argonne National Laboratory, Argonne, IL 60439, USA;

[4]Dipartimento di Fisica, Università di Torino, Torino I-10125, Italy;

[5]INAF−Osservatorio Astrofisico di Torino−Strada Osservatorio 20, Pino Torinese 10025, Italy;

[6]Enrico Fermi Institute, The University of Chicago, Chicago, IL 60637, USA.

ABSTRACT

We present postprocessing AGB nucleosynthesis models with different ^{13}C pockets for zirconium isotopes using new zirconium neutron capture cross-sections from n-TOF measurements. Higher-than-solar ^{92}Zr/^{94}Zr ratios can be obtained by adopting a ^{13}C pocket with a flat profile, which better explains the mainstream SiC grain data from Nicolussi *et al.* (1997) and Barzyk *et al.* (2007), compared to the decreasing ^{13}C profile previously used. The improved agreement between grain data and AGB models provides another piece of evidence to support the previous proposal of a flat ^{13}C profile from an independent study of barium isotopes in mainstream grains. We plan to carry out correlated isotope analysis of barium and zirconium in acid-cleaned mainstream grains in order to better constrain the ^{13}C pocket structures in AGB stars in the future.

Key words: circumstellar matter – meteorites, meteors, meteoroids – nucleosynthesis, abundances – stars: abundances – stars: AGB

1. INTRODUCTION

While nucleosynthetic modeling of Asymptotic Giant Branch (AGB) stars is a straightforward method to study the *s*-process, it requires accurate input data from nuclear physics, e.g., neutron capture probabilities, expressed as the Maxwellian Averaged Cross-Section

(MACS) of each nuclide, and suffers from uncertainties in stellar models, among which the formation of the ^{13}C pocket. Both nuclear and ^{13}C pocket profile uncertainties can be constrained by precise isotopic studies of *s*-process elements in mainstream SiC grains, which are thought to come from low-mass AGB stars (e.g., Zinner *et al.* 1987, Gallino *et al.* 1999, Davis 2011).

Zirconium belongs to the first *s*-process peak and its isotopic abundances are sensitive to AGB stellar conditions. By adopting the MACS values recommended by Bao *et al.* (2000) and the stellar β^- decay rates by Takahashi and Yokoi (1987) in Torino AGB models by Gallino *et al.* (1998), Lugaro *et al.* (2003) (hereafter LDG03) compared model predictions with SiC grain data from Nicolussi *et al.* (1997) and found a satisfactory agreement. Motivated by recent high quality n-TOF zirconium MACS data, Lugaro *et al.* (2014) (hereafter LTK14) reinvestigated zirconium isotope predictions using AGB stellar models by Karakas (2010) with a range of initial stellar mass and metallicity, and found that ^{90,91,96}Zr/^{94}Zr ratios in mainstream grains can be matched, but in the case of ^{92}Zr/^{94}Zr, all predictions are significantly lower than the grain data. LTK14 suggested a smaller ^{92}Zr MACS to explain the mismatch.

Based on new barium isotope data obtained in acid-cleaned mainstream SiC grains, Liu *et al.* (2014) (hereafter LSD14) explored the effect of ^{13}C pocket structures on ^{138}Ba/^{136}Ba and discovered that Torino AGB model predictions of ^{138}Ba/^{136}Ba are extremely sensitive to the structure of the ^{13}C pocket. In order to reach a small group of mainstream grains with low ^{138}Ba/^{136}Ba, a smaller ^{13}C pocket with a flat ^{13}C profile needs to be adopted (see Table 2 of LSD14). In addition, LSD14 found that neutron-magic nuclei (^{88}Sr, ^{138}Ba and ^{208}Pb in particular) are the most sensitive tracers of different ^{13}C pocket structures due to their extremely small MACSs, which makes them act as bottlenecks in the *s*-process path. Inspired by the barium isotope study, we investigated the effect of the ^{13}C pocket on zirconium isotopes in this work. We compare previous mainstream grain data with the Torino AGB models with varying ^{13}C pockets for zirconium isotope ratios, ^{92}Zr/^{94}Zr in particular.

2. GRAIN DATA AND POSTPROCESSING AGB MODELS

We use zirconium isotope abundances in presolar SiC grains previously reported by Nicolussi *et al.* (1997) (renormalized to ^{94}Zr by Davis *et al.* 1999) and Barzyk *et al.* (2007), and include four additional mainstream grains reported by LDG03. All the zirconium isotope data were obtained using the CHARISMA instrument (Resonance Ionization Mass Spectrometry, RIMS) at Argonne National Laboratory (Savina *et al.* 2003). Although the grains in the Nicolussi

et al. study were not analyzed for carbon or silicon isotopes and could not be classified, we assume that the ones with *s*-process zirconium isotopic signatures are mainstream grains. Zirconium isotope data are reported as δ-values, defined as deviation in parts per thousand from isotope ratios measured in grains relative to terrestrial standards. All the grain data are plotted with 2σ uncertainties.

An in-depth description of Torino postprocessing AGB model calculations is given by Gallino *et al.* (1998). Recent updates are reported by Bisterzo *et al.* (2010) and LSD14. The parameters for different ^{13}C pockets discussed in this Letter are given in Table 2 of LSD14. In brief, we did systematic tests with two different ^{13}C pocket structures: Three-zone (hereafter Three-zone model) and Zone-II (hereafter Zone-II model). In the Three-zone case, the pocket is subdivided into three different zones (Zone-I, II & III), while in the Zone-II case only the middle zone (Zone-II) is included. For each structure, the ^{13}C pocket mass and the ^{13}C mass fraction are the two parameters that define a ^{13}C pocket in the models. For a fixed pocket mass, the ^{13}C mass fraction corresponds to the total number of ^{13}C atoms in the pocket and is sometimes referred to in the literature as the ^{13}C efficiency. The ^{13}C efficiency represents a parameterization of the model referred to as a *case*. For example, the ST (standard) case is the ^{13}C efficiency at which the solar *s*-process pattern is well reproduced by averaging 1.5 and 3 $M_{\odot}$ model yields at half solar initial metallicity. The mass fractions of ^{13}C in the D3, D2, D1.5, U1.3 and U2 cases are those in the ST case divided (D) or multiplied (U) by the corresponding factors. To clarify, prior to LSD14, only the Three-zone ^{13}C pocket had been used in the Torino AGB models since Gallino *et al.* (1998).

The AGB stellar mass and metallicity are free parameters in the model, though isotopic data on mainstream grains constrains the parent stars to 1.5−3 $M_{\odot}$ and close-to-solar metallicity (e.g., Barzyk et al. 2007). In this Letter, we compare the grain data with model predictions for a 2 $M_{\odot}$, 0.5 $Z_{\odot}$ AGB star for three reasons: (1) due to effective ^{22}Ne burning in the Torino 3 $M_{\odot}$ AGB model, the predictions agree poorly with the grains for barium isotopes; (2) a 0.5 $Z_{\odot}$ AGB star has more thermal pulses (TPs) and therefore its carbon-rich phase is more extended to cover the whole grain range compared to a 1 $Z_{\odot}$ star (LSD14); (3) the barium isotope data can be well matched by 2 $M_{\odot}$, 0.5 $Z_{\odot}$ Zone-II model predictions (LSD14). We therefore use the same AGB model as LSD14 for zirconium isotopes.

The input parameter MACS is a measure of the reaction rate per pair of interacting particles, defined as $\sigma_{MACS}^{i} = <\sigma^{i} v>/v_T$, where σ^{i} is the (n,γ) cross section of a nuclide *i*, *v* is the relative neutron velocity and v_T is the mean thermal velocity. MACSs are inversely proportional to $1/v_T$ for nuclei between magic neutron numbers because of the $1/v$ behavior of σ^{i}. In addition, σ_{code} is a parameter defined as $\sigma_{MACS}^{i} = <\sigma^{i} v>/v_T$ (30 keV), which better shows departures from $1/v_T$. The σ_{code} values of all zirconium isotopes in the Torino models are reported in Table 1 with comparison to the LDG03 values. For ^{90,91,92,93,94,96}Zr, recent estimates based on n-TOF data are adopted (Tagliente *et al.* 2008a, 2008b, 2010, 2011a, 2011b, 2013). Note that for ^{93}Zr and ^{96}Zr, the recommended MACS values from Bao *et al.* (2000) are confirmed by the recent n-TOF data (Tagliente *et al.* 2011b, 2013). There is an uncertainty of up to a factor of two for the ^{95}Zr MACS (see KADoNiS[1] for details). The ^{95}Zr MACS values used in the Torino models are 50% of that recommended by KADoNiS, in agreement with Toukan & Käppeler (1990); even lower values (~30% of the KADoNiS values) are used in LTK14. As shown in Fig. 1, AGB model predictions of δ^{96}Zr first decrease to its minimum and then increase with pulse numbers due to the activation of the ^{22}Ne neutron source during advanced TPs. By adopting the LTK14 ^{95}Zr MACS in the Torino models, the δ^{96}Zr minimum remains almost unaltered, while for the last TP it decreases by 50‰.

3. COMPARISON OF GRAIN DATA WITH TORINO AGB MODELS WITH THREE-ZONE AND ZONE-II ^{13}C POCKETS

We compared grain data with Three-zone and Zone-II models in Fig. 1. We plot data points for TPs with envelope C/O > 1, which is when SiC grains are expected to condense based on thermodynamic equilibrium calculations (Lodders & Fegley 1995). Three-zone and Zone-II predictions are shown as open and filled symbols, respectively. Good agreement between the grain data and the Three-zone calculations remains for δ^{90}Zr and δ^{91}Zr values. We confirm the conclusion of LDG03 about the minimal impact of ^{89,90}Sr and ^{91}Y branch points on the final abundances of ^{90,91}Zr. Note that discrepant theoretical estimates exist for the MACSs of ^{89,90}Sr and ^{91}Y. The recommended values from Bao et al. (2000) are adopted in the Torino models used in both LDG03 and this study.

[1]KADoNiS: Karlsruhe Astrophysical Data Base of Nucleosynthesis in Stars, website http://www.kadonis.org/, version v0.3;

LTK14 concluded that the values of $\delta^{92}Zr \geq -50‰$ observed in some grains cannot be reached by their new AGB models or by FRUITY[2] models (Cristallo *et al.* 2009, 2011). These grains also cannot be matched by the Torino Three-zone model (in Fig. 1). The production of ^{92}Zr and ^{94}Zr is unaffected by branching effects because different neutron capture paths flowing through branch points in this region all join at ^{92}Zr. However, as also noticed by LDG03, the ^{92}Zr abundance is affected by the marginal activation of the $^{22}Ne(\alpha,n)^{25}Mg$ reaction during the TPs. The sensitivity to this second neutron source can be ascribed to the fact that the ^{92}Zr MACS deviates from $1/v_T$, as can be clearly seen in Table 1, whereas the MACS of ^{94}Zr closely follows the $1/v_T$ rule. For reference, in Fig. 2 $\delta^{92}Zr$ decreases by ~50‰ by decreasing the $^{22}Ne(\alpha,n)^{25}Mg$ rate from K94[3] to ½×K94 rate. This rate has been constrained to lie between ¼×K94 and K94 rate by LSD14. Using the lowest rate (¼×K94) lowers the $\delta^{92}Zr$ Three-zone model predictions by 100‰, and makes the disagreement with the grains with $\delta^{92}Zr \geq -50‰$ even more problematic. Interestingly, by switching to the Zone-II ^{13}C pocket, the same model predicts a wider range of $\delta^{90,91,92}Zr$ values, with the D1.5 case reaching most of the grains with $\delta^{92}Zr \geq -50‰$. Good agreement remains for $\delta^{90,91}Zr$ values. All zirconium isotope ratios are affected by different ^{13}C pockets, and the higher $\delta^{92}Zr$ values can be matched by AGB models with the Zone-II ^{13}C pocket using the new n-TOF ^{92}Zr MACS.

The grains with the highest $\delta^{96}Zr$ values cannot be matched by either the Three-zone or the Zone-II models (Fig. 1). Due to its small MACS, the amount of ^{96}Zr destroyed by radiative neutron capture is negligible. Consequently, ^{96}Zr production linearly depends on the ^{95}Zr neutron capture rate (and therefore on the ^{95}Zr MACS value) at 23 keV during the marginal activation of the $^{22}Ne(\alpha,n)^{25}Mg$ reaction in the more advanced TPs, where the peak neutron density reaches $\sim 10^{10}$ cm^{-3}. Thus, model predictions of $\delta^{96}Zr$ are strongly affected by the $^{22}Ne(\alpha,n)^{25}Mg$ reaction. The higher the reaction rate, the higher the $^{95}Zr_n/^{95}Zr_{\beta-}$ ratio, and in turn, the higher the ^{96}Zr abundance ($^{95}Zr_n$ and $^{95}Zr_{\beta-}$ are the numbers of ^{95}Zr capturing a neutron and undergoing β^- decay, respectively). As the upper limit K94 rate is adopted in all the model calculations in Fig. 1, the possibility of a higher $^{22}Ne(\alpha,n)^{25}Mg$ rate to explain the higher $\delta^{96}Zr$ is excluded. Instead, the mismatch with the grain data could be caused by: (1) solar zirconium contamination in these particular SiC grains; (2) a larger ^{95}Zr MACS; and/or (3) their parent AGB stars having lower

[2]FRUITY, Full-network Repository of Updated Isotopic Tables & Yields, website http://fruity.oa-teramo.inaf.it/.
[3]K94: the lower limit of the $^{22}Ne(\alpha,n)^{25}Mg$ reaction rate recommended by Käppeler et al. (1994). Unless noted otherwise, the K94 rate is adopted in model calculations.

mass and higher metallicity than we have investigated. Although a larger ^{95}Zr MACS is plausible considering its current uncertainty, it will result in the overproduction of ^{96}Zr compared to its solar *s*-process abundance (Bisterzo *et al.* 2011).

3. DISCUSSION

3.1 Effects of the ^{13}C Pocket Structure on Zirconium Isotope Ratios

AGB model predictions suffer from uncertainties in the ^{13}C neutron source, which depends on free parameters like the adopted ^{13}C pocket profile and mass (Gallino *et al.* 1998). In *s*-process nucleosynthesis, MACSs of most of the nuclei between magic numbers likely follow $1/v_T$ behavior and are therefore relatively insensitive to the ^{13}C neutron source. As can be seen in Table 1, ^{92}Zr is an exception as its MACS deviates from $1/v_T$ by 30% from 8 keV to 23 keV, while ^{94}Zr strictly follows this rule. Thus, ^{92}Zr/^{94}Zr can be used to constrain the ^{13}C neutron source. We did a systematic search for the difference between calculations with Three-zone and Zone-II ^{13}C pockets by varying the pocket mass parameter. Calculations were done with a range of pocket masses: for Three-zone models, from Three-zone_d2 ($4.7\times10^{-4}\,M_\odot$) to Three-zone_p2 ($18.7\times10^{-4}\,M_\odot$); for Zone-II models, from Zone-II_d2.5 ($2.1\times10^{-4}\,M_\odot$) to Zone-II_p2 ($10.6\times10^{-4}\,M_\odot$).

Zirconium overproduction factors for the D1.5 case are given in Table 2. The corresponding δ^{92}Zr model predictions are plotted against ^{13}C pocket mass in Fig. 2 to show the overall higher δ^{92}Zr values in Zone-II models. The models that agree with the grain data are shown in Fig. 3. Three-zone_d2 is an exception as both ^{92}Zr and ^{94}Zr are nearly equally overproduced in this model. In addition, we found that δ^{92}Zr values for each ^{13}C efficiency in both the Three-zone and Zone-II calculations decrease with increasing ^{13}C pocket mass on average, as shown in Fig. 2. For reference, the δ^{92}Zr maximum in the D1.5 case drops by ~60‰ from Zone-II_d2.5 to Zone-II_p2, and by ~50‰ from Three-zone_d2 to Three-zone according to Fig. 1 & Fig. 3. This trend results from the fact that ^{94}Zr has a smaller MACS than ^{92}Zr, and can be accumulated more effectively with increasing ^{13}C pocket mass.

3.2 Effects of ^{92}Zr and ^{94}Zr MACS Uncertainties on Zirconium Isotope Ratios

We evaluated the effect of the 1σ uncertainties in the ^{92}Zr and ^{94}Zr MACSs in Table 1 on the predicted δ^{92}Zr values. For Three-zone calculations, the maximum δ^{92}Zr in the ST case decreases by 50‰ by adopting the upper limit (UL) ^{92}Zr MACS or the lower limit (LL) ^{94}Zr

MACS; it increases by 60‰ by adopting the LL ^{92}Zr MACS or the UL ^{94}Zr MACS. Due to the MACS uncertainties, we are not able to exclude the possibility of a lower ^{92}Zr MACS and/or a higher ^{94}Zr MACS to explain the mismatch by the LTK14, FRUITY, and Three-zone models for $\delta^{92}Zr \geq -50$‰. For instance, by adopting both the LL ^{92}Zr MACS and the UL ^{94}Zr MACS, the Three-zone model predictions Fig. 1 will be shifted by ~100‰ in the y-axis and a better agreement could be obtained with the grains. Therefore, better determination of the ^{92}Zr and ^{94}Zr MACSs ($2\sigma < 5\%$) is needed to reduce the model uncertainty and to determine the necessity of the Zone-II models.

On the other hand, thanks to the well-determined MACSs of ^{136}Ba and ^{138}Ba, and the barium isotope data of acid-cleaned mainstream grains, LSD14 were able to demonstrate that the ST cases in the Zone-II_d2.5 to Zone-II models are required to explain $\delta(^{138}Ba/^{136}Ba)$ values < −400‰ in a minor group of mainstream grains. The fact that all the Zone-II models agree better with the δ^{92}Zr values in grains than the Three-zone models do strongly supports the existence of smaller ^{13}C pockets with flat ^{13}C profiles in the parent stars of mainstream grains. Although Zone-II models can explain the whole range of $\delta(^{138}Ba/^{136}Ba)$ values observed by LSD14, we cannot exclude the possibility of different ^{13}C pockets existing in their parent stars because only the ones with $\delta(^{138}Ba/^{136}Ba) < -400$‰ require the Zone-II ^{13}C pocket. What percentages of the parent AGB stars have Zone-II ^{13}C pockets therefore remains an open question. Correlated isotopic data for zirconium and barium in mainstream grains will help to answer this question. The measurements in acid-cleaned mainstream grains will be done soon to investigate the correlation between δ^{92}Zr and δ^{138}Ba values and to further test our constraint on the ^{13}C pocket.

4. CONCLUSION

The better agreement of zirconium isotope data, $\delta^{92}Zr \geq -50$‰ in particular, in mainstream SiC gains with the Torino Zone-II AGB model calculations strongly supports our previous proposal of a small (i.e., mass less than 5.3×10^{-4} $M_{\odot}$) Zone-II ^{13}C pocket to explain $\delta^{138}Ba < -400$‰ in some mainstream grains. While ^{94}Zr is always more overproduced than ^{92}Zr in most Three-zone models, all the Zone-II models explored so far are able to more or less equally overproduce ^{92}Zr and ^{94}Zr, which explains the higher δ^{92}Zr predictions by the Zone-II models. A general trend of decreasing δ^{92}Zr values with increasing pocket mass is observed, which is caused by the higher overproduction of ^{94}Zr. Due to the uncertainty in zirconium MACSs, we cannot completely exclude Three-zone models in explaining existing grain data.

MACSs of ^{92,94}Zr with smaller uncertainties are needed to clarify this point. The sensitivity of δ^{92}Zr and δ^{138}Ba values to different ^{13}C pocket structures provides an opportunity to place more stringent constraints on the ^{13}C pockets of mainstream grain parent stars by measuring correlated zirconium and barium isotopes. Acid-cleaned mainstream grains will be analyzed to exclude the possibility of solar zirconium contamination in the grains. Comparison of acid-cleaned grain data with AGB model predictions with reduced uncertainties for both zirconium and barium isotopes will eventually shed light onto the longstanding puzzle of the shape and the size of the ^{13}C pocket.

Acknowledgements: Part of the Torino model numerical calculations has been sustained by the B2FH Association (http://www.b2fh.org/). NL acknowledges the NASA Earth and Space Sciences Fellowship Program (NNX11AN63H) for support. This work was also supported by the NASA Cosmochemistry program through grant NNX09AG39G (to AMD). SB acknowledges financial support from the Joint Institute for Nuclear Astrophysics (JINA, University of Notre Dame, USA) and from Karlsruhe Institute of Technology (KIT, Karlsruhe, Germany).

REFERENCES

Bao, Z. Y., Beer, H., Käppeler, F., et al. 2000, At. Data. Nucl. Data Tables, 76, 70

Barzyk, J. G., Savina, M. R., Davis, A. M., et al. 2007, Meteorit. Planet. Sci., 42, 1103

Bisterzo, S., Gallino, R., Straniero, O., Cristallo, S. & Käppeler, F. 2010, MNRAS, 404, 1529

Bisterzo, S., Gallino, R., Straniero, O., Cristallo, S. & Käppeler, F. 2011, MNRAS, 418, 284

Cristallo, S., Straniero, O., Gallino, R., et al. 2009, ApJ, 696, 797

Cristallo, S., Piersanti, L., Straniero, O., et al. 2011, ApJS, 197, 17

Davis, A. M. 2011, Proc. Natl. Acad. Sci. USA, 108, 48, 19142

Davis A. M., Nicolussi G. K., Pellin M. J., et al. (1999) In Nuclei in the Cosmos V (ed. N. Prantzos & S. Harissopulos), Editions Frontières, Paris, 563–566

Gallino, R., Arlandini, C., Busso, M., et al. 1998, ApJ, 497, 388

Gallino, R., Busso, M., Picchio, G. & Raiteri, C. M. 1990, Nature, 348, 298

Käppeler, F., Wiescher, M., Giesen, U., et al. 1994, ApJ, 437, 396

Karakas, A. I. 2010, MNRAS, 403, 1413

Liu, N., Savina, M. R., Davis, A. M., et al. 2013, ApJ, submitted

Lodders, K. & Fegley, B. Jr. 1995, Meteoritics, 30, 661

Lugaro, M., Davis, A. M., Gallino, R., et al. 2003, ApJ, 593, 486

Lugaro, M., Tagliente, G., Karakas, A. I., et al. 2013, ApJ, 780, 95

Nicolussi, G. K., Davis, A. M., Pellin, M. J., et al. 1997, Science, 277, 1281

Savina, M. R., Pellin, M. J., Tripa, C. E., et al. 2003, GCA, 67, 3215

Tagliente, G., Fujii, K., Milazzo, P. M., et al. 2008a, Phys. Rev. C, 77, 035802

Tagliente, G., Fujii, K., Milazzo, P. M., et al. 2008b, Phys. Rev. C, 78, 045804

Tagliente, G., Milazzo, P. M., Fujii, K., et al. 2010, Phys. Rev. C, 81, 055801

Tagliente, G., Milazzo, P. M., Fujii, K., et al. 2011a, Phys. Rev. C, 84, 015801

Tagliente, G., Milazzo, P. M., Fujii, K., et al. 2011b, Phys. Rev. C, 84, 055802

Tagliente, G., Milazzo, P. M., Fujii, K., et al. 2013, Phys. Rev. C, 87, 014622

Takahashi, K. & Yokoi, K. 1987, At. Data. Nucl. Data Tables, 36, 375

Toukan, K. & Käppeler, F. 1990, ApJ, 348, 357

Zinner, E., Ming, T. & Anders, E. 1987, Nature, 330, 730

FIGURE CAPTIONS

Figure 1 Three-isotope plots of $\delta(^{90}Zr/^{94}Zr)$, $\delta(^{91}Zr/^{94}Zr)$ and $\delta(^{92}Zr/^{94}Zr)$ versus $\delta(^{96}Zr/^{94}Zr)$. The grain data from Nicolussi *et al.* (1997) (renormalized by Davis *et al.* 1999) and Barzyk et al. (2007) are compared to Three-zone (left, open symbols) and Zone-II (right, filled symbols) AGB model predictions for a 2 $M_{\odot}$, 0.5 $Z_{\odot}$ AGB star with a range of ^{13}C efficiencies. The entire evolution of the AGB envelope composition is shown, but symbols are plotted only when C > O. Uncertainties in the grain data are ±2σ. Dotted lines represent solar zirconium isotope ratios.

Figure 2 The $\delta(^{92}Zr/^{94}Zr)$ model predictions for a 2 $M_{\odot}$, 0.5 $Z_{\odot}$ AGB star from Table 2 are plotted against ^{13}C pocket mass for Three-zone and Zone-II ^{13}C pockets.

Figure 3 Three-isotope plots of $\delta(^{92}Zr/^{94}Zr)$ versus $\delta(^{96}Zr/^{94}Zr)$. The same grain data from Fig. 1 are compared to different model predictions for a 2 $M_{\odot}$, 0.5 $Z_{\odot}$ AGB star with a range of ^{13}C mass fraction within each pocket. The masses of Zone-II_d2.5, Zone-II_p2 and Three-zone_d2 ^{13}C pockets are 2.1×10^{-4} $M_{\odot}$, 9.37×10^{-4} $M_{\odot}$ and 10.6×10^{-4} $M_{\odot}$, respectively.

Table 1 Zirconium Neutron Capture Cross Sections, $\sigma_{code} = \langle \sigma v \rangle / v_T$ (30 keV) (mbarn)

Isotope	LDG03[a]				This work[b]			
	8 keV	23 keV	30 keV	1σ err (30 keV)	8 keV	23 keV	30 keV	1σ err (30 keV)
^{90}Zr	18.9	20.8	21.0	9.5%	18.1	18.8	19.3	4.7%
^{91}Zr	90.5	64.7	60.0	13.3%	87.3	67.4	63.0	6.3%
^{92}Zr	47.2	34.6	33.0	12.1%	50.1	38.5	38.0	8.0%
^{93}Zr	128.0	103.0	95.0	10.5%	127.9	102.8	95.0	9.4%
^{94}Zr	30.1	26.6	26.0	3.8%	30.2	29.8	30.5	6.5%
^{95}Zr*	111.1	85.2	79.0	15.0%	55.5	42.6	39.5	15.0%
^{96}Zr	18.1	11.1	10.7	4.7%	17.2	10.9	10.3	6.0%

Notes: [a] Lugaro *et al.* (2003) and references therein;

[b] See text for the references;

*The 1σ uncertainty is only based on the theoretical estimate from Bao *et al.* (2000).

Table 2 Overproduction Factors of Zirconium Isotopes in the Envelope at the 7th (C = O) and 25th Pulses (the last one)

7th pulse	Three zone _d2	Three zone	Three zone _p2	Zone-II _d2.5	Zone-II _d2	Zone-II	Zone-II _p2
^{90}Zr	2.623	4.550	7.313	2.169	2.443	4.017	6.094
^{91}Zr	2.612	4.558	7.414	2.155	2.426	3.990	6.042
^{92}Zr	2.478	4.316	7.127	2.044	2.289	3.712	5.549
^{94}Zr	2.735	5.064	8.969	2.167	2.445	4.088	6.177
^{96}Zr	1.032	1.081	1.174	1.020	1.026	1.058	1.105
25th pulse							
^{90}Zr	11.135	22.598	37.694	8.226	9.852	18.899	30.205
^{91}Zr	12.611	25.850	43.346	9.252	11.100	21.402	33.939
^{92}Zr	11.520	23.889	40.816	8.360	10.011	19.265	30.344
^{94}Zr	12.213	26.847	49.468	8.354	10.047	19.831	32.260
^{96}Zr	4.342	8.340	13.200	3.248	3.740	6.566	9.389

Note: The results are from 2 $M_{\odot}$, 0.5 $Z_{\odot}$ AGB model calculations in the D1.5 case. The reference masses of Three-zone and Zone-II ^{13}C pockets are $9.37\times10^{-4}\ M_{\odot}$ and $5.3\times10^{-4}\ M_{\odot}$, respectively. The mass of the ^{13}C pocket for each column is the reference mass multiplied (p) or divided (d) by the corresponding factor.

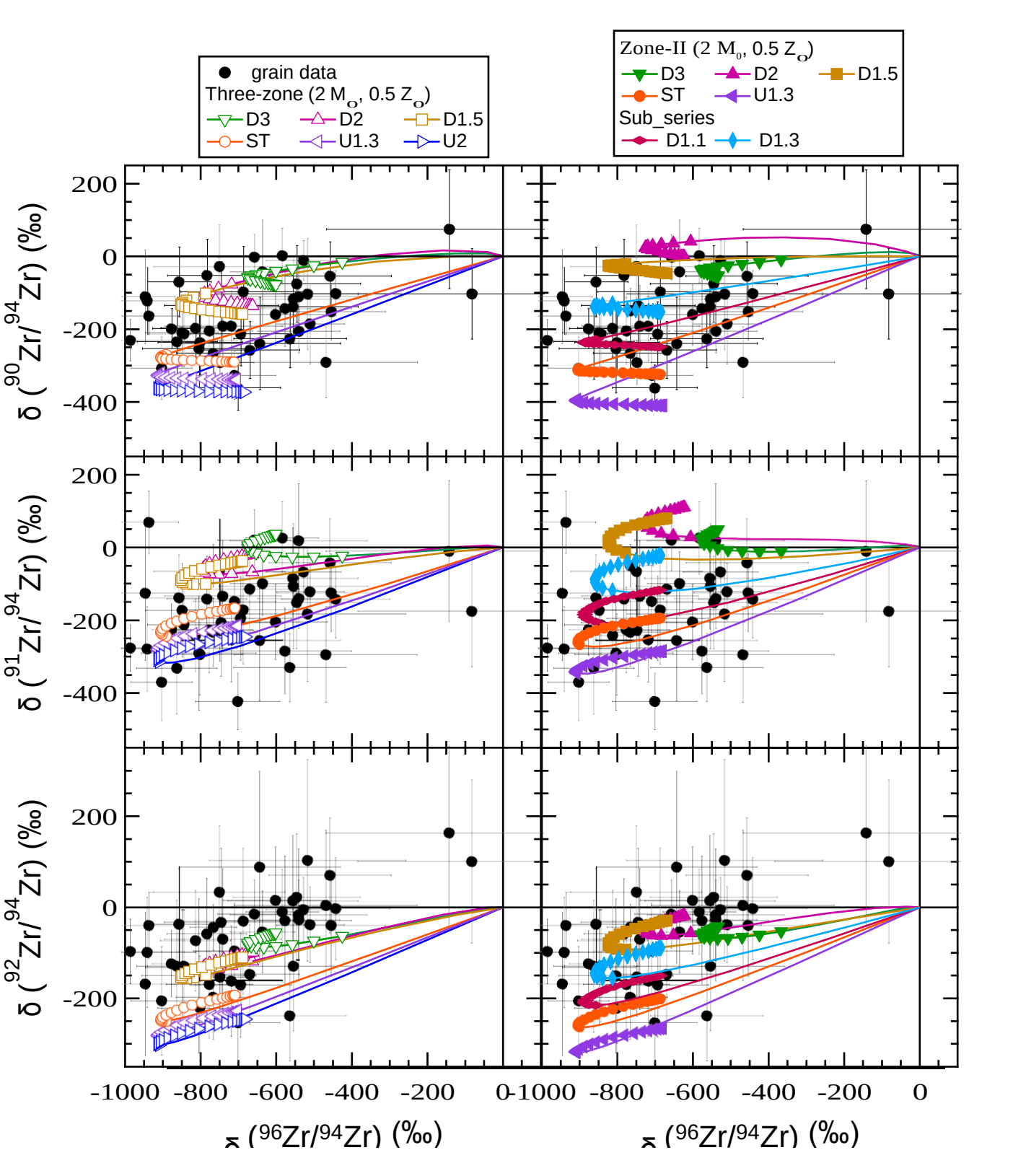
grain data
Three-zone (2 M$_o$, 0.5 Z$_o$)
D3
D2
D1.5
ST
U1.3
U2
Zone-II (2 M$_o$, 0.5 Z$_o$)
D3
D2
D1.5
ST
U1.3
Sub_series
D1.1
D1.3
δ (^{90}Zr/^{94}Zr) (‰)
δ (^{91}Zr/^{94}Zr) (‰)
δ (^{92}Zr/^{94}Zr) (‰)
δ (^{96}Zr/^{94}Zr) (‰)
200
0
-200
-400
-1000
-800
-600
-400
-200
0

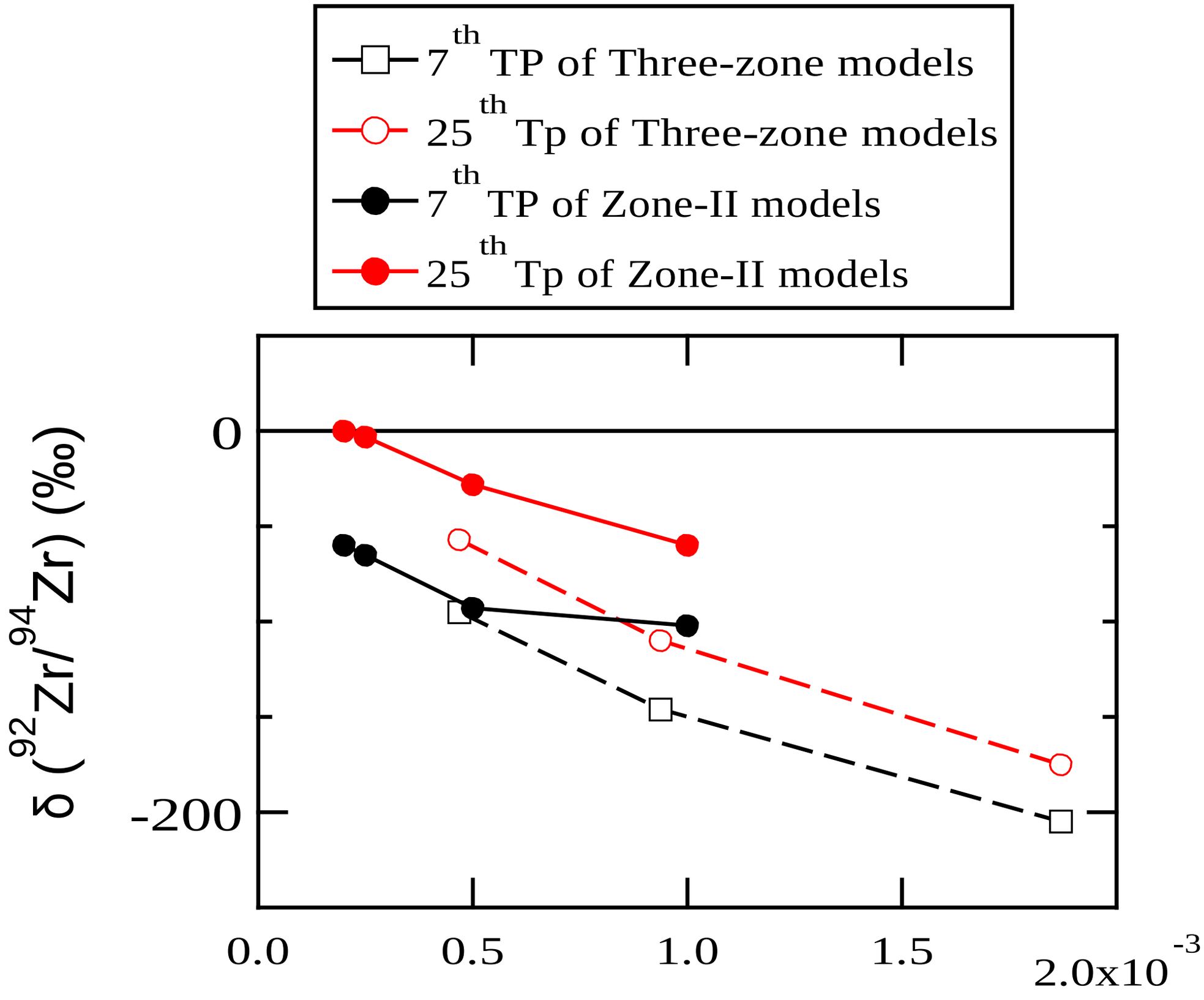
7th TP of Three-zone models
25th Tp of Three-zone models
7th TP of Zone-II models
25th Tp of Zone-II models
0
-200
δ (92Zr/94Zr) (‰)
0.0
0.5
1.0
1.5
2.0x10-3

^{13}C pocket mass (M)

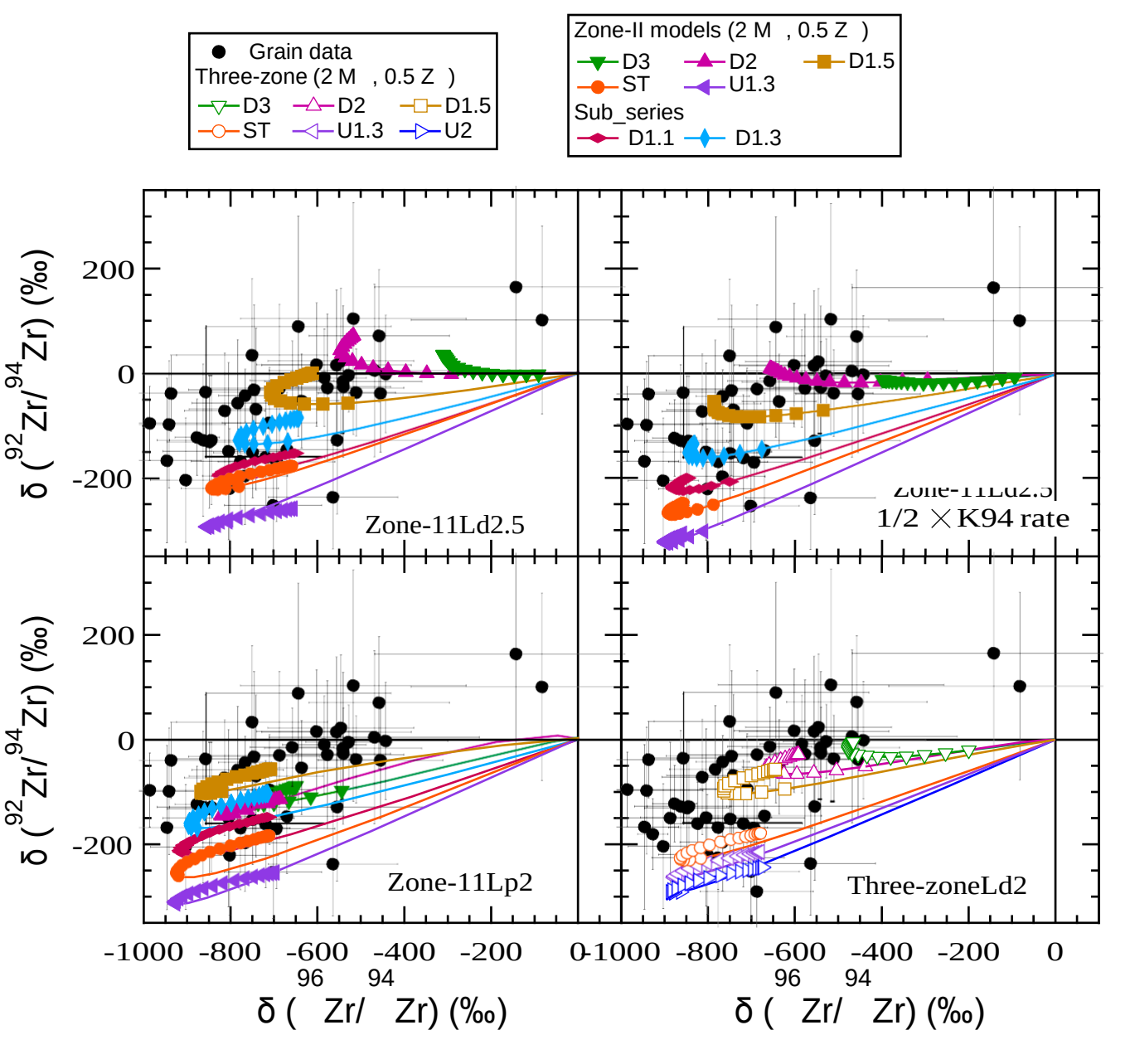
Grain data
Three-zone (2 M , 0.5 Z)
D3
D2
D1.5
ST
U1.3
U2
Zone-II models (2 M , 0.5 Z)
D3
D2
D1.5
ST
U1.3
Sub_series
D1.1
D1.3
Zone-11Ld2.5
1/2 × K94 rate
Zone-11Lp2
Three-zoneLd2
δ (92Zr/ 94Zr) (‰)
δ (96Zr/ 94Zr) (‰)
200
0
-200
-1000
-800
-600
-400
-200
0